ACS NANO

Article

Direct Plasmon-Accelerated Electrochemical Reaction on Gold Nanoparticles

Chen Wang, Xing-Guo Nie, Yi Shi, Yue Zhou, Jing-Juan Xu, Xing-Hua Xia, and Hong-Yuan Chen

ACS Nano, **Just Accepted Manuscript** • Publication Date (Web): 11 May 2017

Just Accepted

ACS Publications

ACS Nano is published by the American Chemical Society. 1155 Sixteenth Street N.W., Washington, DC 20036

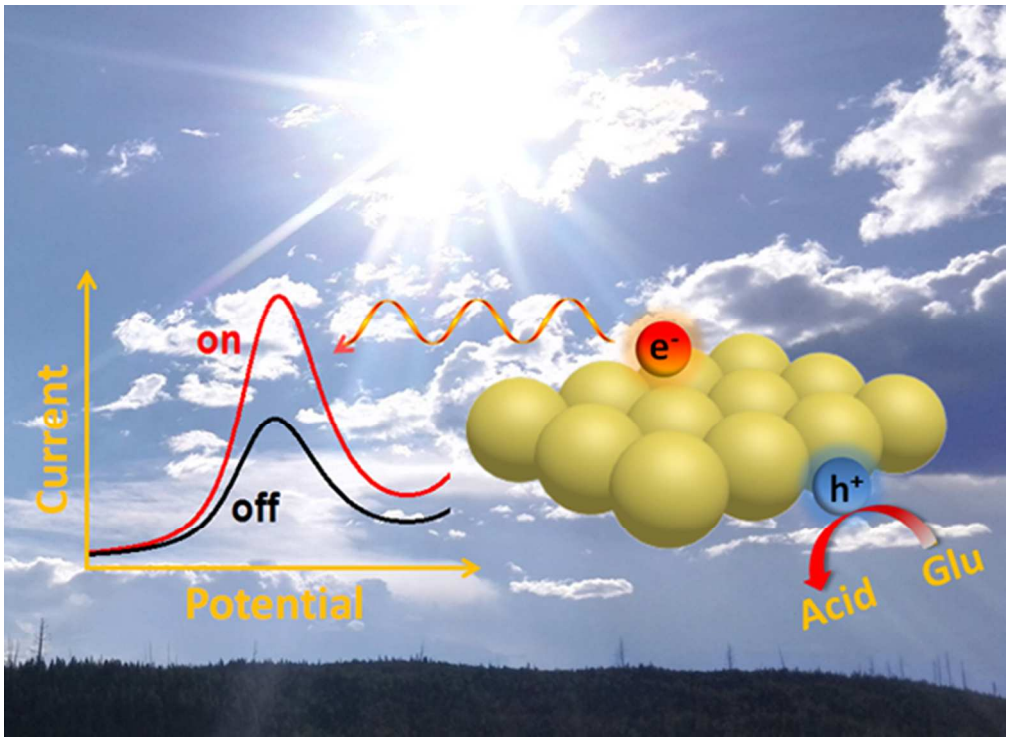

Graphic abstract

54x39mm (300 x 300 DPI)

Direct Plasmon-Accelerated Electrochemical Reaction on Gold Nanoparticles

Chen Wang,[†,‡] *Xing-Guo Nie,*[†,‡] *Yi Shi,* [†] *Yue Zhou,* [†] *Jing-Juan Xu,*[†] *Xing-Hua Xia,*[†]* *Hong-Yuan Chen*[†]

†State Key Laboratory of Analytical Chemistry for Life Science and Collaborative Innovation Center of Chemistry for Life Sciences, School of Chemistry and Chemical Engineering, Nanjing University, Nanjing 210093, China.

‡Key Laboratory of Biomedical Functional Materials, School of Science, China Pharmaceutical University, Nanjing, 211198, China

*To whom correspondence should be addressed. E-mail: xhxia@nju.edu.cn (X.H.X)

ABSTRACT Direct photocatalysis making use of plasmonic metals has attracted significant attention due to the light harnessing capabilities of these materials associated with localized surface plasmon resonance (LSPR) features. Thus far, most reported work has been limited to plasmon-induced chemical transformations. Herein, we demonstrate that electrochemical reactions can also be accelerated by plasmonic nanoparticles upon LSPR excitation. Using glucose electrocatalysis as a model reaction system, the direct plasmon-accelerated electrochemical reaction (PAER) on gold nanoparticles (AuNPs) is observed. The wavelength- and solution-pH-dependent electrochemical oxidation rate and the dark-field scattering spectroscopy results confirm that the

hot charge carriers generated during plasmon decay are responsible for the enhanced electrocatalysis performance. Based on the proposed PAER mechanism, a plasmon-improved glucose electrochemical sensor is constructed, demonstrating the enhanced performance of the non-enzyme sensor upon LSPR excitation. This plasmon-accelerated electrochemistry promises potential applications in (bio)electrochemical energy conversion, electroanalysis and electrochemical devices.

KEYWORDS: plasmonics · hot electrons · electrochemical reaction · gold nanoparticles · glucose

Plasmonic nanoparticles are characterized by their well-known surface catalytic properties and strong light-matter interactions.[1] The excitation of localized surface plasmon resonance (LSPR) occurs when a discontinuous nanostructured material with high free-electron mobility (Ag, Au, Cu, *etc*.) interacts with photons that match the resonance energy of the collective oscillation of the surface valence electrons.[2] As a result of LSPR excitation, a strong electromagnetic field and a high concentration of energetic charge carriers (electron-hole pairs) are generated at the nanostructured surface.[3-5] The enhanced electromagnetic field make the plasmonic nanoparticles ideal platforms for many applications, including surface-enhanced Raman spectroscopy,[6,7] solar cells,[8] single-molecule spectroscopy,[9] biomolecular sensing,[10] and many others.[11,12] Recently, experimental and theoretical studies have revealed that optically excited plasmonic nanoparticles can concentrate and channel the energy of visible light into adsorbed molecules, activating and accelerating chemical transformations directly on their surfaces.[13-15] This photocatalysis process exhibits fundamentally different behavior from phonon-driven thermal processes, offering an alternative family of photochemical transformations.

Plasmon-accelerated chemical transformation through LSPR excitation was first observed in the photocatalytic degradation of the volatile organic compound HCHO on gold nanoparticles (AuNPs).[16] The reaction rate exhibited a strong dependence on the wavelength of light, suggesting that the excitation of LSPR was responsible for the observed photocatalytic activity. In addition to the organic compound degradation, it was recently found that Ag nanocubes could harvest visible light to directly drive the catalytic oxidation reactions of ethylene epoxidation, CO and NH_3 through LSPR excitation.[17,18] Similarly, the dissociation of H_2 was accomplished using AuNPs supported on SiO_2.[19] Although no electron transfer between AuNPs and the support was observed, the dissociation rate was almost 2 orders of magnitude higher than that observed on AuNPs/TiO_2.[19,20] More recently, the direct photocatalysis of water splitting on AuNPs was realized using a plasmonic photoelectrode.[21] The photocurrent was generated by direct electron transfer from the AuNPs to protons in water. Since there was no semiconductor in the catalyst, a Schottky barrier was avoided for the photocatalysis, and a higher collected efficiency for hot charge carriers was achieved. These experimental results confirm that plasmonic metals can act as light absorbers and catalytic sites, effectively harvesting light for chemical transformations. The mechanism of LSPR-assisted chemical reactions was investigated using surface-enhanced Raman spectroscopy[22] and dark-field scattering spectroscopy.[23] It was suggested that a great number of energetic charge carriers would be generated on the surface of nanostructures upon LSPR excitation. The photocatalytic reaction rate is then enhanced by injection of the energetic charge carriers to the accessible orbitals of the adsorbed molecule before they dissipate into phonon modes.[3,4,17-22]

Harnessing the energy from hot charge carriers of plasmonic nanostructures is a promising research area for energy conversion and photocatalysis. Up until now, there has been a growing number of examples of hot charge carriers mediating photochemistry, including the dissociation

of gas molecules,[19,20] selective oxidation,[17] direct reduction,[24] organic synthesis[25] and organic compound decomposition.[16] So far, most attention has been focused on the plasmonics mediating chemical transformations. There have been a few reports on direct plasmonics enhancing electrochemical reactions. The progress achieved in the direct photocatalysis for chemical reactions on plasmonic nanostructures has inspired our great interest to investigate this plasmonic effect on electrocatalytic processes. Herein, the direct plasmon-accelerated electrochemical reaction (PAER) on AuNPs was investigated using glucose electrocatalysis as a model system. Upon LSPR excitation, energetic charge carriers are generated on the AuNPs surface. Under suitable voltage bias, the generated hot holes can be effectively depleted by the oxidation of glucose due to their matched energy levels. This process effectively inhibits the recombination of hot electrons with hot holes. Thus, the generated hot electrons are driven to the external circuit, producing observable current. In this process, many hot holes will be used for glucose electrochemical oxidation. In addition, since the PAER system is Schottky-junction-free, the hot charge carriers can be harnessed more efficiently, which ensures the occurrence of highly efficient PAER on AuNPs toward glucose electrooxidation.

RESULTS AND DISCUSSION

AuNPs were prepared through the thermal reduction of $HAuCl_4$ by sodium citrate.[26] The resultant 15-nm spherical AuNPs show an LSPR absorption at 521 nm, as characterized by TEM (Fig. 1a) and UV-vis spectroscopy (Fig. 1b). Since a glassy carbon (GC) electrode shows a much lower light response than a gold disk electrode (Fig. S1 in the supporting information), it is an ideal substrate to study the plasmonic effects of AuNPs. After deposition of the AuNPs on a GC electrode, the spherical structure of the AuNPs remained, as shown by the SEM image in Fig. 1c. However, a minor redshift in the UV-vis absorbance spectrum appeared when the AuNPs were

deposited on the GC support (Fig. S2 in the supporting information), which may be due to the change of the dielectric environments. The factors influencing the optical properties of AuNPs will be discussed in detail in the following section.

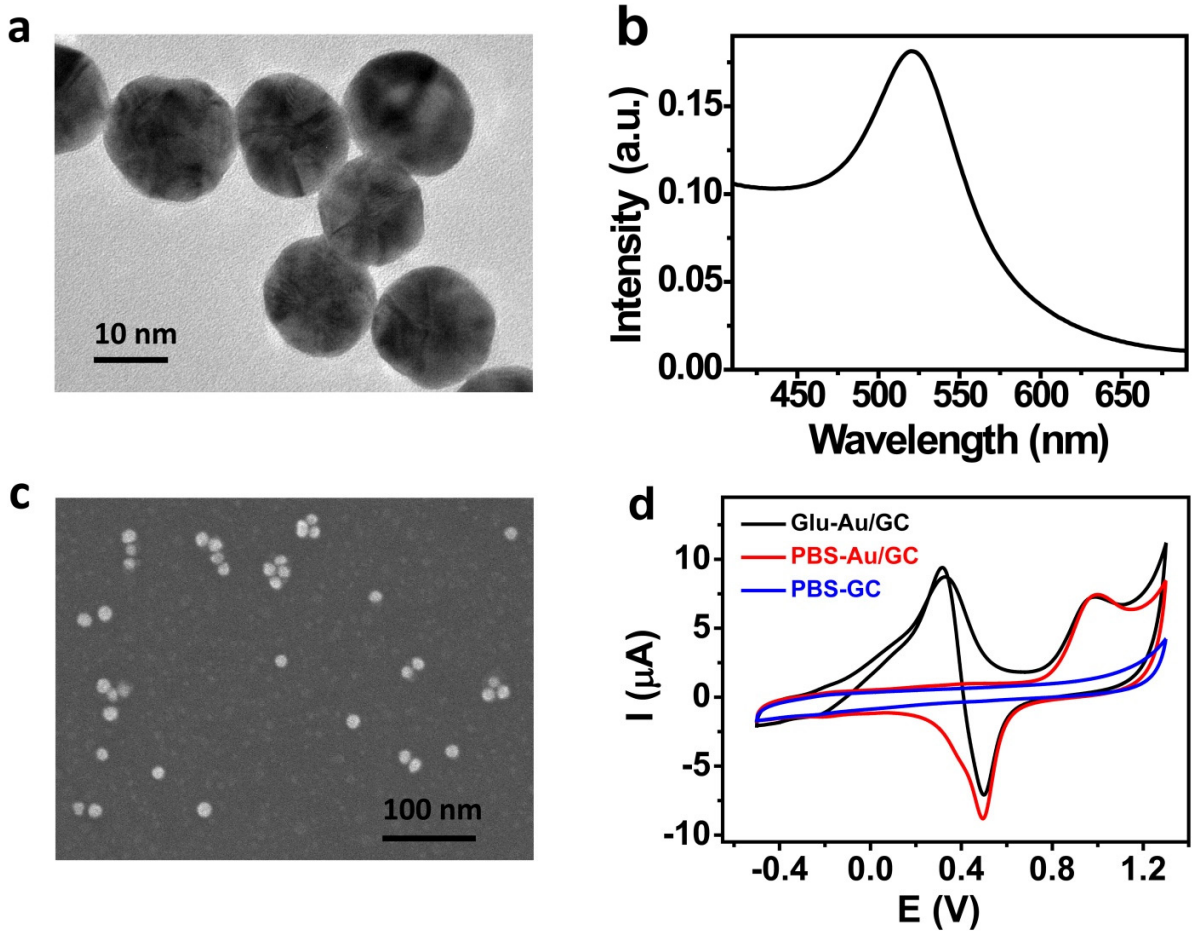

Figure 1. Characterizations of the AuNPs and AuNPs/GC electrode. (a) TEM image of the prepared 15-nm AuNPs. (b) UV–vis extinction spectrum of a dilute aqueous solution of 15-nm AuNPs. (c) SEM image of the AuNPs deposited on a GC support. (d) CV of 100 mM glucose (black curve) in 100 mM PBS buffer (pH 7.4) on an AuNPs/GC electrode at a scan rate of 50 mV/s. For comparison, CVs of an AuNPs/GC (red curve) and a naked GC electrode (blue curve) in 100 mM PBS (pH 7.4) under the same conditions are also displayed.

The electrocatalytic activity of AuNPs (15 nm) toward glucose oxidation was investigated in 100 mM PBS (pH 7.4) containing 100 mM glucose at 25 °C. The cyclic voltammogram (CV) of a GC electrode in PBS supporting electrolyte shows a featureless curve (Fig. 1d, blue curve) in a broad potential window from -0.5 V to 1.3 V. The one for the AuNPs (red curve) displays the typical characteristics for a gold electrode, showing gold oxide formation and reduction. When glucose is added to the solution, significant anodic current peaks for glucose electrocatalytic oxidation in both the forward and reverse potential scans are observed on the AuNPs/GC electrode (Fig. 1d, black curve). To signify the plasmonic effects on the electrocatalytic oxidation of glucose, the forward potential scan for glucose oxidation on the AuNPs/GC electrode in a range from 0 V to 0.8 V was studied (the complete CVs of glucose are shown to Fig. S3 in the supporting information). As shown in Fig. 2a, a well-defined anodic peak for the oxidation of glucose appears in the dark. Upon illumination of the AuNPs/GC electrode by a 532-nm light source with a total maximum intensity of 200 mW cm^{-2}, an obvious enhancement in the anodic current is observed (Fig. 2a, red curve). The peak current is about 2-fold larger than that in the dark (from 1.01 μA to 2.05 μA). This increase in electrochemical current indicates fast injection of electrons from gold to the external circuit, which can be clearly seen from the steady-state photocurrent changes measured at a constant potential of 0.4 V (*vs.* Ag/AgCl) upon LSPR excitation of the AuNPs (Fig. 2b). When LSPR excitation occurs, a sharp increase in the anodic current occurs and then disappears quickly as the light source is switched off. A slight decrease in the anodic current response during continuous on/off switching appears, which is possibly caused by the poisoning effect due to the adsorption of the reaction product (gluconic acid) on the AuNPs.[27,28] The control experiment was performed using Au disk electrode instead of AuNPs/GC electrode. The result

shown in Fig. S4 indicates a relative weak photo effect of Au disk as compared to the AuNPs catalyst. The reaction product was identified using high-performance liquid chromatography mass spectrometry (Fig. S5). As indicated, the observed quasi-molecular ion band at m/z 195 agrees with the spectrum of ion fragments of the gluconic acid standard sample. The quantity of reaction product formed under 532-nm illumination for 40 min was more than the one in the dark.

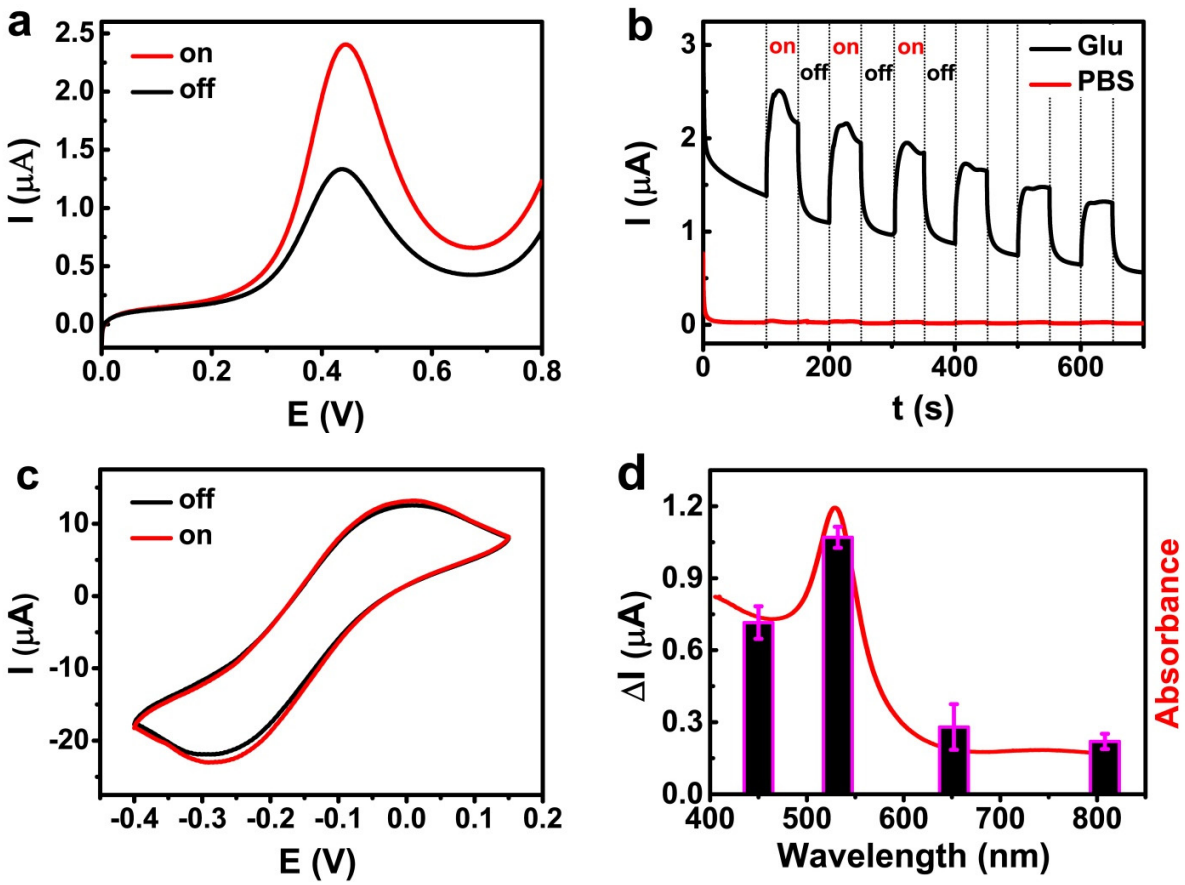

Figure 2. Plasmon-enhanced electrocatalytic oxidation. (a) Forward scan curves of CVs for glucose (100 mM in 100 mM PBS, pH 7.4) oxidation on the AuNPs (15 nm)/GC electrode with and without LSPR excitation (532 nm, 200 mW/cm^2). The potential scan rate was 50 mV/s. (Red curve = light on; black curve = light off). (b) *I-t* curves at 0.4 V (*vs.* Ag/AgCl) with LSPR excitation

on and off in the presence (black trace) and absence of 100 mM glucose (red trace). (c) CVs of 2 mM $Ru(NH_3)_6Cl_3$ on the AuNPs/GC electrode at 298.15 K at a scan rate of 50 mV/s with (red curve) and without (black curve) LSPR excitation. (d) Wavelength-dependent peak currents for glucose oxidation at 0.43 V (black column), and LSPR spectrum (red solid line) of the 15-nm AuNPs (529 nm).

To understand the origin of the current enhancement, the electrochemistry of a $Ru(NH_3)_6Cl_3$ probe with reversible redox chemistry was studied at different temperatures (Fig. 2c and Fig. S6a). A pair of well-defined redox peaks with peak potentials at -0.01 V and -0.26 V were observed in the CVs with and without LSPR excitation (532 nm), respectively. Upon light illumination, no obvious change in the electrochemistry of $Ru(NH_3)_6Cl_3$ was observed (red curve, Fig. 2c and Fig. S6a). This confirms that a temperature-dependent electrochemical response of this electrochemical probe exists. As shown in Fig. S6b, the electrochemical responses in the dark increase with an increase of the solution temperature due to heat-accelerated mass transport. Light irradiation did not affect the peak current significantly at each selected temperature. These results demonstrate that the heat effect is relatively weaker than the plasmonic effect under the present experimental conditions. Experimental and theoretical studies have shown that under illumination of solar intensity (100 mW/cm^2), the maximum transient temperature increases by only ~0.01 K by plasmonic heating.[4] According to the vant Hoff Rule, the reaction rate would become double with a 10 K increase of the reaction system. Therefore, an illumination intensity of 10^6 mW/cm^2 could only produce a 2-fold increase in reaction rate by the plasmonic heating.[14,17] In our system, the maximum illumination intensity was 400 mW/cm^2, the contribution from plasmonic heating in oxidation current should not be significant. Then, we measured the excitation-wavelength-

dependent steady-state currents of glucose oxidation on the AuNPs/GC electrode at 0.43 V to understand the plasmon-accelerated effect. As shown in Fig. 2d, the steady-state current changes significantly with the wavelength (black column), showing a similar trend with the LSPR spectrum of the AuNPs (red line). The maximum current value is observed under 532-nm illumination, which nearly overlaps with the plasmonic excitation peak of the 15-nm AuNPs (529 nm in Fig. S2), suggesting that LSPR excitation should be the main factor responsible for the observed current increase, which is in good agreement with previous reports.[17,18] Thus, we attribute the dramatic enhancement in anodic current of glucose electrooxidation to the LSPR effect of the AuNPs.

The experimental results in Fig. 2 enable us to suggest a possible mechanism for the enhanced electrocatalytic performance on plasmonic metals. In the case of AuNPs, the electrons are filled in the *d*-band. Upon LSPR excitation, electrons oscillate collectively, leading to interband excitation. This process gives enough energy for electrons to move to active states above the Fermi level of the AuNPs.[29,30] The electron energy distribution in the AuNPs before and after LSPR excitation is schematically illustrated in Fig. S7.[5,31] The excited energetic charges of the electrons and holes (referred to as “hot electrons” and “hot holes”) resulting from plasmon-induced charge separation are concentrated on the AuNPs surface. The generated hot electrons will deviate away from the electron equilibrium state in the AuNPs and may have three probable transfer channels, as illustrated in Fig. 3a: (i) recombining with holes; (ii) directly participating in the electrochemical reaction; and (iii) being transferred into the external circuit driven by a voltage bias if the holes are removed. We propose that under suitable voltage bias the generated hot holes can be driven to the surface to assist the oxidation of glucose due to their matched energy levels. This process can effectively inhibit the recombination of hot electrons with hot holes (channel i). With the driving force of the positive potential (above the onset potential), hot electrons will be driven into the

external circuit (channel iii), while the hot holes will be driven to the surface for glucose oxidation, leading to enhanced current for glucose electrooxidation. The principle of PAER and the setup is illustrated in Fig. 3b. Based on the proposed PAER mechanism, the hot hole yield (the ratio of the generated hot holes number to the illumination photons) is estimated as 0.00658% using the method described in the supporting information and results in Fig. S8.

To verify the proposed PAER mechanism, the effect of excitation intensity on the electrocatalytic performance was studied. We found that the plasmon-enhanced electrocatalytic activity of the AuNPs dramatically increased with the illumination intensity up to ~300 mW cm^{-2}, and then, a transition from a linear to super-linear dependence above ~300 mW cm^{-2} appeared (Fig. 3c). A similar dependence of the reaction rate for photocatalytic ethylene epoxidation on the illumination intensity has been previously reported on a Ag plasmonic structure,[18] which proves to be a signature of hot charge carriers related to photochemical reactions, revealing more production of hot charge carriers at a higher illumination intensity. In addition, the generality of the proposed PAER for ascorbic acid (AA), ethanol (EtOH), ethylene glycol (EG) and glycerol (Gly) was also confirmed. Similar PAER behaviors for these reactants were observed in the steady-state currents with LSPR excitation on and off (Fig. 3d), demonstrating that the direct LSPR-accelerated electrochemical reaction is a general phenomenon of plasmonic nanostructures.

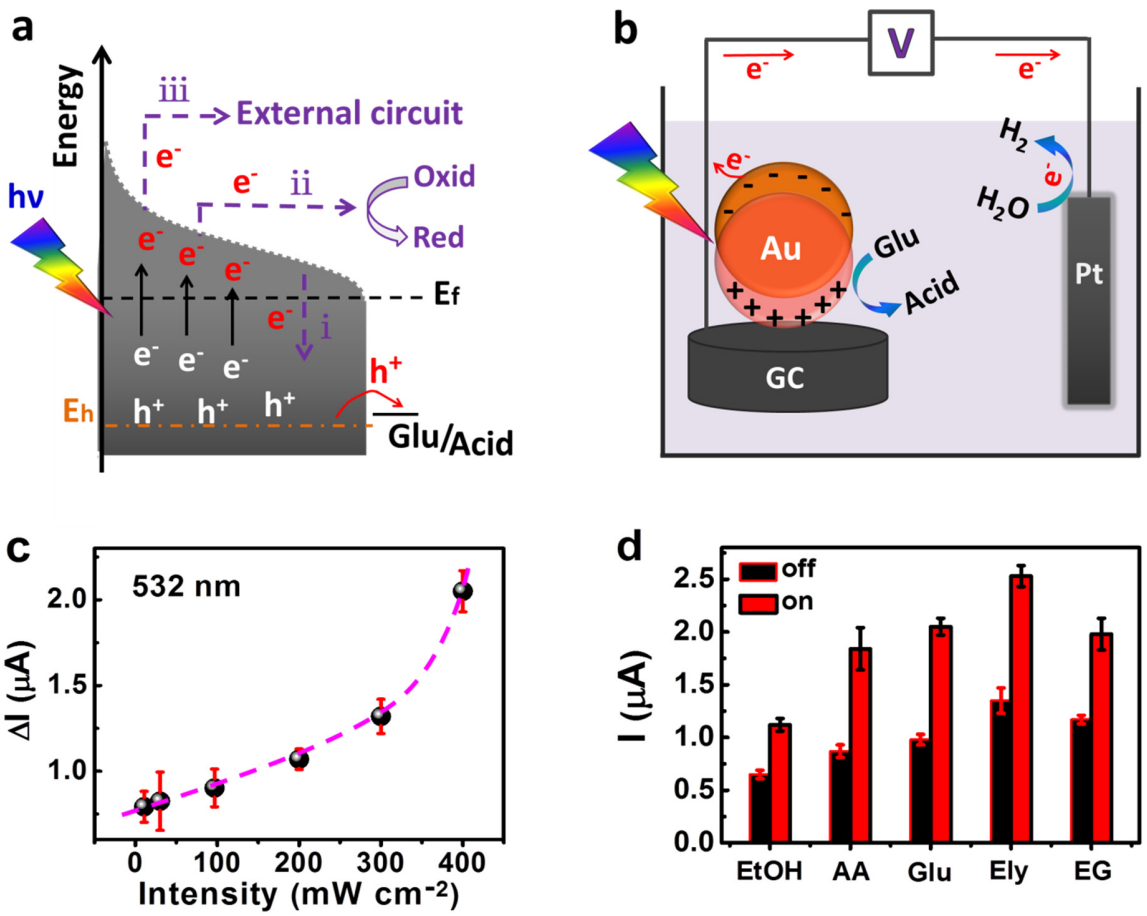

Figure 3. Mechanism of PAER on the AuNPs. (a) Possible transfer channels of LSPR-excited hot charge carriers. The dashed yellow line indicates the energy level (E_h) of the hot holes. (b) Illustration of the electrochemical setup and the principle of PAER. (c) Peak currents at 0.43 V for the electrocatalytic oxidation of 100 mM glucose as a function of irradiation intensity of the 532-nm light source. (d) The generality of the proposed PAER mechanism toward different electrochemical reactions. The concentrations of glucose and ascorbic acid in PBS were 100 mM, whereas ethanol, ethylene glycol and glycerol in PBS had a volume ratio of 10 % (relative to PBS).

It is well-known that the optical properties of plasmonic metal nanoparticles can be influenced by many factors, such as the dielectric constants of the metal, the size and shape of the particles,

and the surroundings. If any of these factors changes, a shift in the LSPR spectrum (LSPRS) will occur.[32] To obtain direct evidence of the hot charge carrier transfer process, a dark field spectroscopy integrated with electrochemistry technique was established in our laboratory, which allows us to collect LSPRS of a single AuNP under potential control. Fig. 4a illustrates the setup of the *in situ* electrochemical LSPRS (photo of the apparatus is shown in Fig. S9). As we know, upon LSPR excitation, plasmons relax through two pathways: photon scattering or formation of energetic charge carriers. Smaller nanoparticles are more favorable for producing higher energy charge carriers, while larger particles tend to decay through photon scattering.[14] Herein, as a demonstration, 50-nm AuNPs were modified on an indium-tin-oxide (ITO) slide for LSPRS investigation. At the open-circuit potential (OCP), the 50-nm AuNPs appear as green color dots in the dark-field image (Fig. 4b, inset shows the amplified image), and an LSPR scattering peak appears at 551 nm, which is approximately redshifted by 20 nm compared to the absorbance peak in solution (532 nm) due to the energy dissipation and substrate effect.[33] When glucose is added (final concentration of 100 mM in 100 mM PBS), the LSPR scattering peak shows a blueshift of ~8.0 nm at the OCP upon 20-min illumination (Fig. 4c, red curve) due to the change of the dielectric environment with the addition of glucose. When a positive potential of +0.4 V is applied to the AuNP, a redshift of ~7.5 nm in the LSPR scattering peak is observed (Fig. 4c, green curve). This shift reflects the electron density of the AuNP returning to its initial state, which is caused by the discharge of excess electrons from the AuNP to the external circuit through the applied positive potential. These electrochemical LSPRS results prove the formation of energetic charge carriers in LSPR, confirming the proposed PAER mechanism.

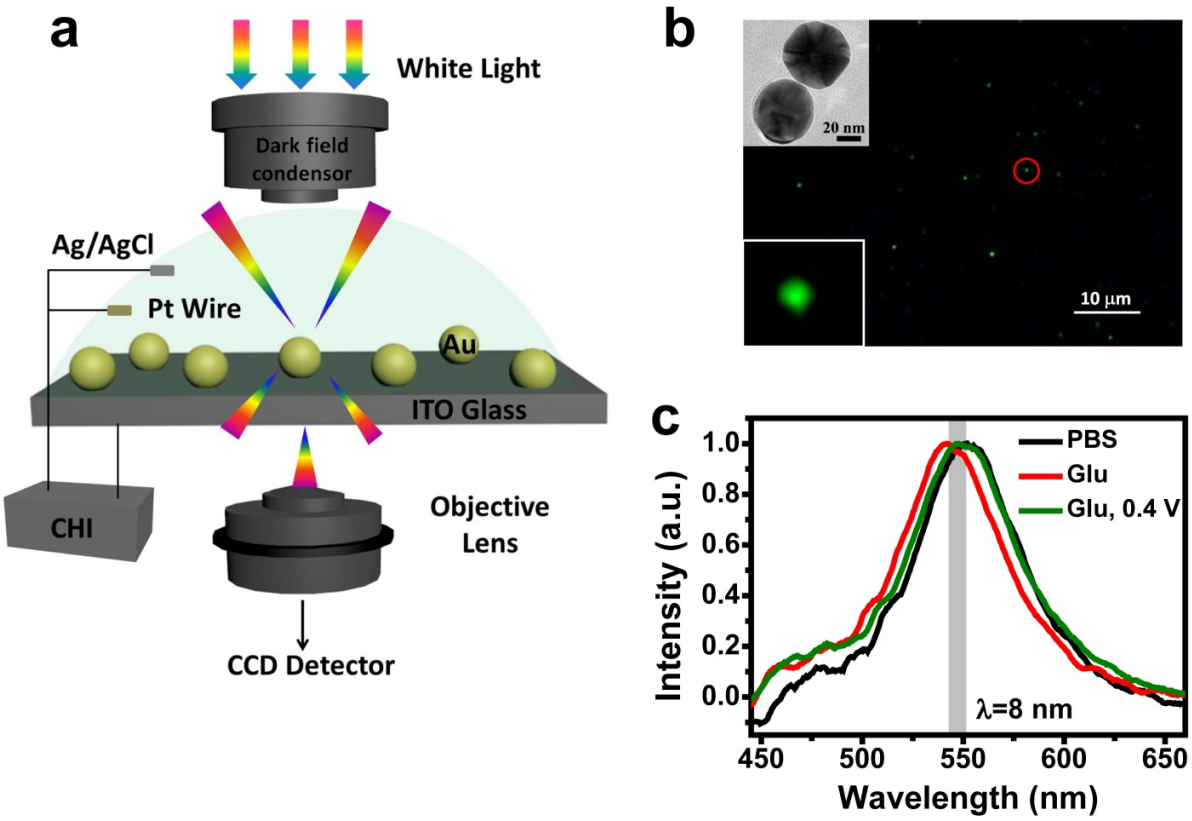

Figure 4. LSPR scattering spectroscopy. (a) Schematic apparatus for the *in situ* electrochemical LSPR scattering spectroscopy measurement in 100 mM PBS (pH 7.4) under a dark-field microscope. The electrochemical cell consists of a Pt wire as the auxiliary electrode, a Ag/AgCl wire as the reference and AuNP-modified ITO as the working electrode. (b) Dark-field image of the AuNPs deposited on ITO in 100 mM PBS (scale bar: 10 μm). The inset shows the TEM and amplified dark-field images of the 50-nm AuNPs. (c) LSPRS of a single AuNP on the ITO electrode in different medium (the LSPRS intensity is normalized). Black line: 100 mM PBS at the OCP; red line: 100 mM glucose in 100 mM PBS (pH 7.4) at the OCP; green line: 100 mM glucose in 100 mM PBS at 0.4 V.

The size of the plasmonic metal has a profound influence on the efficient formation of the energetic charge carriers.[5,31,34] In this work, AuNPs with different diameters of 5, 10, 15, 25, and

50 nm were chosen to investigate the size effect of the plasmonic metal on PAER. UV-vis absorption spectra and TEM images are shown in Fig. S10 in the supporting information. The UV-vis absorption spectra show a blueshift from 532 nm to 516 nm with a decrease of the AuNPs diameter from 50 nm to 5 nm. CVs of glucose on the AuNPs with different diameters are displayed in Fig. 5a. To estimate the size effect on the electrocatalytic activity, the current densities for different electrodes were calculated using the real surface area (determined by the charge passed through the reduction peak between 0.8 V and 1.2 V in the CVs in 0.5 M H_2SO_4, as shown in Fig. S11 and Table S1), as shown in the inset of Fig. 5b, which are averaged from six parallel measurements with relative standard deviations of less than 4.1%. The normalized current densities show a minor fluctuation range (from 0.88 to 1.0) for the AuNPs with different sizes, suggesting similar electrocatalytic activities of the different sized AuNPs toward glucose oxidation. However, the increased current density (ΔJ) upon LSPR excitation for different AuNPs/GC electrodes shows a particle-size-dependent trend (Fig. 5b). The ΔJ increases with a decrease of the AuNPs size from 50 nm to 10 nm. However, the situation is reversed for the smallest AuNPs (5 nm). Theoretical studies have shown that a significant number of hot charge carriers with higher energies can be generated for small plasmonic nanocrystals upon optical excitation.[5,31] In contrast, for large nanocrystals, most of the generated hot electrons have small energies (very close to the Fermi level), and thus, the number of highly excited energetic carriers is relatively less. Therefore, more highly energetic carriers can be generated with smaller AuNPs. However, smaller particles show a decreased in extinction cross section, which will compete with the size-dependent hot charge carrier concentration and may lead to anomalous behavior of the 5-nm AuNPs in this work.

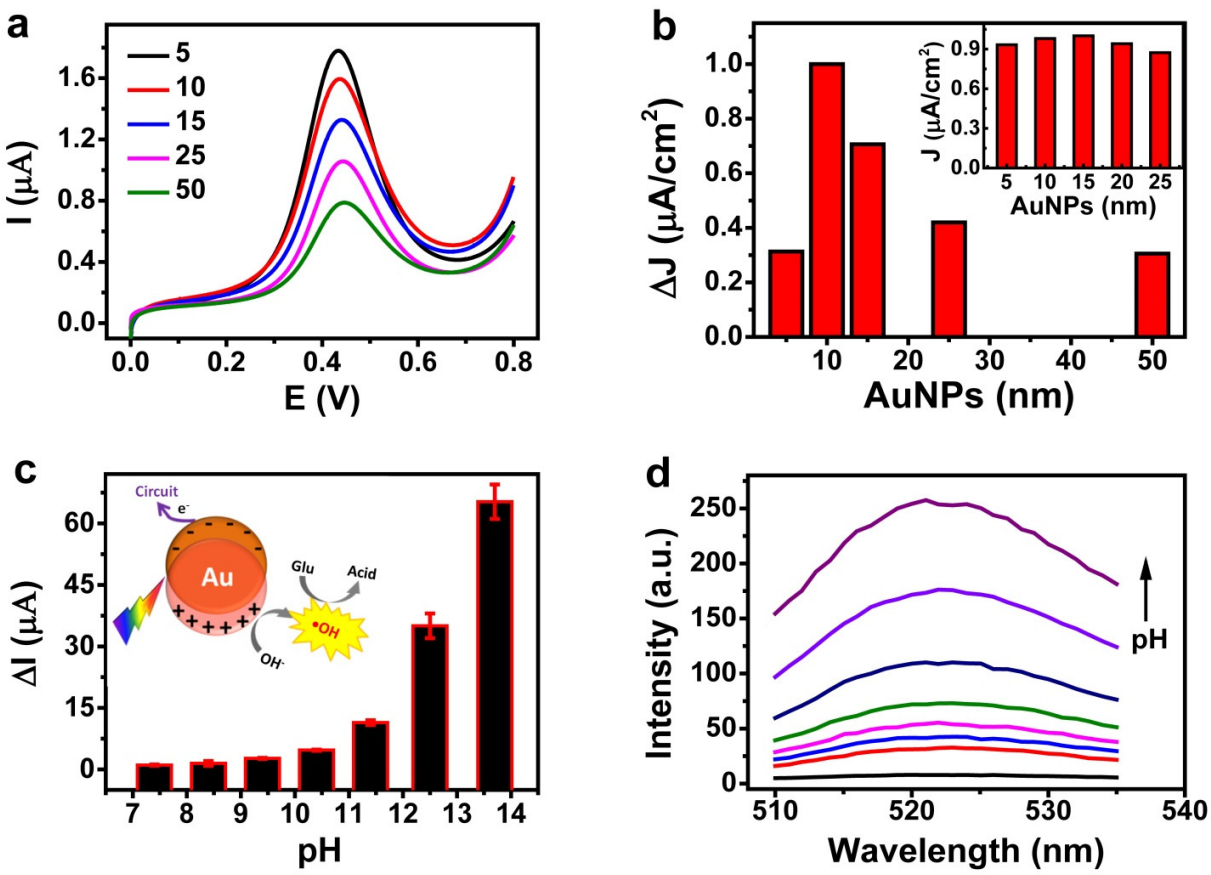

Figure 5. Effect of the size of AuNPs and pH on PAER. (a) CVs of glucose (100 mM in 100 mM PBS, pH 7.4) oxidation on the AuNP-modified GC electrodes at a scan rate of 50 mV/s (AuNPs are 5-50 nm in diameter). (b) The enhanced current density (ΔJ) upon LSPR excitation *versus* the diameter of the AuNPs. The inset shows the current density of glucose oxidation on the AuNP-modified electrodes with different particle sizes in the dark. (c) Influence of solution pH on the peak current for glucose oxidation on the AuNPs (15 nm) with LSPR excitation on and off. (d) Fluorescence spectra of DCF (product of the reaction of DCDHF with •OH) taken after 40 min of LSPR excitation in different pH systems (from bottom to up: 7.4, 8.4, 9.4, 10.4, 11.4, 12.4, and 13.7). The excitation wavelength was 500 nm.

The influence of the solution pH on the increased peak currents (ΔI) was investigated with LSPR excitation on and off. As presented in Fig. 5c, the peak current increases gradually when the solution pH increases from pH 7.4 to 10.4, then increases exponentially from pH 11.4 to 13.7. Due to this striking result, we suggest a different glucose oxidation mechanism in highly alkaline conditions, which depends on the generation of hydroxyl radicals through photoexcitation (Fig. 5c, inset). It has been demonstrated that in highly alkaline conditions, large quantities of small-sized hydroxyl anions (OH^-) can easily diffuse to the nanoparticle surface.[35] Owing to the high oxidation capacity of hot holes, OH^- can be easily oxidized into •OH radicals, which can easily diffuse through solution to oxidize glucose with a faster rate. Therefore, in highly alkaline conditions, hot holes can be scavenged with much more quickly than in neutral conditions. The recombination probability of hot electrons with holes in channel (i) is efficiently declined. An increased number of hot electrons can be transferred from the AuNPs into the external circuit, resulting in a much larger anodic current. Supporting evidence for the proposed mechanism was provided by the detection of •OH radicals using a fluorescent probe. The characteristic photoluminescence (PL) at 521 nm of 2',7'-dichlorofluorescein (DCF) was used, which is the product of the reaction of the fluorescent probe 2',7'-dichlorodihydrofluorescein (DCDHF) with an •OH radical.[36,37] As shown in Fig. 5d, a significant increase in the fluorescence intensity at 521 nm appears with an increase of the solution pH, indicating a faster formation rate of •OH radicals in the alkaline conditions, which is in good agreement with the increase of the electrochemical current. At pH 13.7, the fluorescence peak intensity increases sharply, which is caused by the continuous production of •OH radicals and the accumulation of the fluorescent derivative DCF.

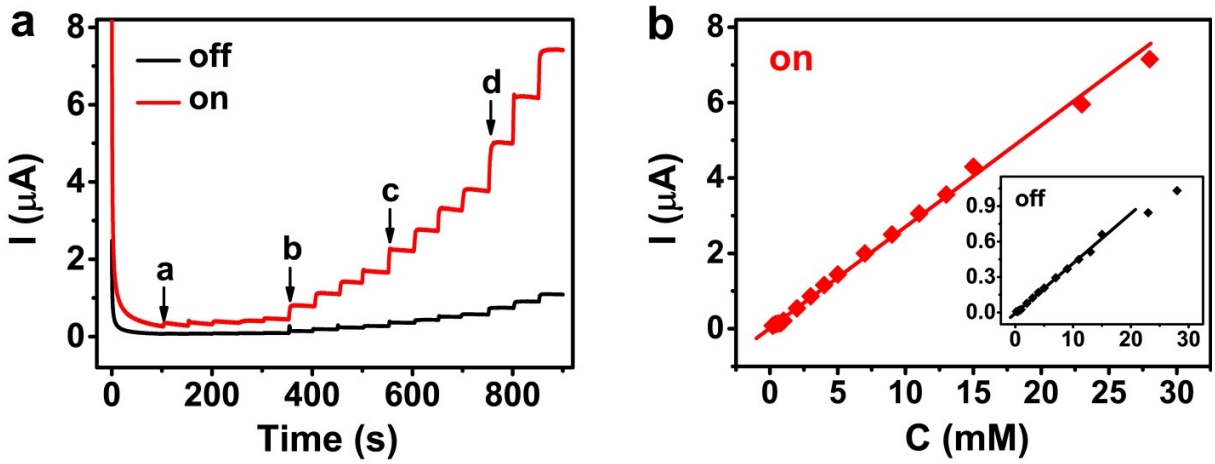

Figure 6. Plasmon-enhanced glucose sensor. (a) *I-t* curves for glucose oxidation in 0.1 M NaOH on the AuNPs/GC electrode at 0.3 V (*vs.* Ag/AgCl). Black curve: in dark; Red curve: LSPR excitation. (b) The corresponding calibration plot of the glucose sensor with LSPR excitation on. The inset shows the calibration plot in the dark. Glucose was successively injected into stirred 0.1 M NaOH with 0.2 mM (a), 1 mM (b), 2 mM (c), and 5 mM (d) glucose.

Since the electrochemical reaction can be accelerated by the LSPR effect, chemical or biological sensors based on LSPR excitation should have improved performance, *i.e.*, a higher detection sensitivity and a lower detection limit. As a demonstration, a glucose non-enzymatic biosensor using this simple AuNPs/GC electrode was constructed based on the PAER mechanism. Amperometric detection of glucose with LSPR excitation on and off was conducted on an AuNPs/GC electrode at 0.3 V in 0.1 M NaOH (Fig. 6a). When the sensor is conducted in the dark, a continuous but minor increase in current is observed upon injection of glucose at regular intervals (black curve in Fig. 6a). In comparison, when LSPR excitation is on, the current increases much more rapidly upon the addition of glucose (red curve in Fig. 6a). The corresponding calibration

curve is shown in Fig. 6b, showing a detection sensitivity of 0.95 μA cm^{-2} mM^{-1} within the linear range of 0.2-23 mM and a detection limit of 9.0 μM at a signal to noise ratio of 3. On the contrary, the glucose sensor showed a shortened linear range (0.2-15 mM) with a detection sensitivity of 0.15 μA cm^{-2} mM^{-1} and a detection limit of 60.0 μM (inset in Fig. 6b) in the dark, which is a more than 6 times lower detection sensitivity than LSPR excitation. The results imply that noble metal nanostructures upon LSPR excitation can be applied in sensitive and robust biological or chemical sensing. However, due to the poisoning effect or possible evolution of AuNPs, there are still some limitations need to be addressed in detection. The poisoning effect can be eliminated using electrochemical activation. The effect due to evolution of gold nanoparticles cannot be avoided for all the catalytic systems. More work needs to be performed on the proposed LSPR enhanced sensors in the future.

CONCLUSION

In summary, our work has demonstrated that plasmonic AuNPs can accelerate the electrocatalytic oxidation of glucose. By investigating the effect of the LSPR wavelength, light intensity, and heat effect on the enhancement of glucose oxidation, a PAER mechanism was proposed. Upon LSPR excitation, energetic charge carriers are generated during plasmon decay. Under suitable voltage bias, hot holes can assist the electrocatalytic oxidation of glucose due to their matched energy levels, while hot electrons are driven into the external circuit, producing observable current. The results of a single-particle scattering spectroscopy with electrochemistry technique further confirm the proposed PAER mechanism. The effects of the size of AuNPs size and solution pH on glucose oxidation were also investigated. Interestingly, in highly alkaline conditions, a much larger change in anodic current appears, which is caused by faster scavenging of hot holes by OH^-. The present work endeavors to shed light on the LSPR enhancement

mechanism toward electrochemical reactions and provide insights into designing electrochemical devices and assays using plasmonic metals.

MATERIALS AND METHODS

Reagents. Glucose, gluconic acid, 2',7'-dichlorodihydrofluorescein (DCDHF), and ascorbic acid (AA) were purchased from Sigma and used as received. NaOH, KCl, ethanol (EtOH), ethylene glycol (EG), glycerol (Gly), sodium citrate, tannic acid, and potassium carbonate were purchased from Nanjing Chemical Reagent Co., Ltd. (Nanjing, China). $HAuCl_4 \cdot 4H_2O$ was purchased from the First Regent Factory (Shanghai, China). All aqueous solutions were prepared with Millipore water (resistivity of 18.2 MΩ·cm). Indium-tin-oxide (ITO) glass (≤ 10 Ω/sq) was purchased from Zhuhai Kaivo Optoelectronic Technology Co., Ltd. (China).

Synthesis of AuNPs. Citrate-stabilized gold nanoparticles (AuNPs) were prepared through the thermal reduction of $HAuCl_4$ by sodium citrate according to the classic Frens method.[26] For the synthesis of AuNPs with different diameters (10-50 nm), 100 ml of 0.01% (weight percent) $HAuCl_4$ was heated to boiling, and then, 1-5 ml of 1% (weight percent) sodium citrate was immediately added into the boiling solution under rapid stirring. The reactants remained boiling for 7-8 min. During this time, the solution color changed to deep red. AuNPs with 5 nm diameters were synthesized by the reduction of chloroauric acid using tannic acid and citrate.[38] Briefly, solutions of A and B were first prepared as follows. For solution A, 4 ml of sodium citrate (1%), 0.7 ml of tannic acid (1%), 0.2 ml of potassium carbonate (0.1 M) and 15.1 ml of H_2O were combined. For solution B, 1 ml of $HAuCl_4$ solution (1%) and 79 ml of H_2O were combined. Then, the two solutions were kept at 60 °C for at least 2 min before mixing. The mixed solution was then heated to boiling for 7-10 min until color changed from clear to deep red. All the AuNP solutions

were cooled to room temperature with continuous stirring. The AuNP dispersions were stored at 4 °C and centrifugalized at 3000 rpm for 18 min before use.

Characterizations. UV-vis adsorption spectroscopic characterization was performed using a Nanodrop-2000C spectrophotometer (Thermo Fisher Scientific Inc). The morphologies of the samples were characterized using transmission electron microscopy (TEM, JEM-2100, Japan) by drying a droplet of the sample solutions on Ni-grids with carbon films. Scanning electron microscopic (SEM) images were acquired on silicon wafers by an S-4800 (Japan).

Experimental setup. Electrochemical measurements with illumination on and off were carried out on a CHI 660E instrument (Chenhua, China) under steady-state conditions at 25 °C. A working electrode was made by drop-casting 10 μL of the catalysts to cover the glassy carbon electrode (3-mm diameter), forming the AuNPs/GC electrodes. A platinum wire was used as the counter electrode. An Ag/AgCl electrode was used as the reference for all the electrochemical tests. Visible light sources of 450, 532, 652, and 808 nm were used. All experiments for glucose oxidation and $Ru(NH_3)_6Cl_3$ electrochemistry were performed under a N_2 atmosphere.

Characterization of the reaction product by HPLC-MS. Analysis was performed by an HPLC/MS instrument on an Agilent 1290/6460 Triple Quad LC/MS. A Waters XBridge BEH Amide Column (2.1 mm x 50 mm x 2.5 μm) was used. The mobile phase consisted of water containing 0.05% ammonia (A) and acetonitrile (B) at a flow rate of 0.8 ml/min using the following gradient: 0.0-1.0 min, 85% solvent B; 1.0-7.0 min, 85%-25% solvent B; 7.0-8.0 min, 25% solvent B; 8.0-8.2 min, 25%-85% solvent B; and 8.2-12.0 min, 85% solvent B. The injection volume was 10 ul. MS analysis was performed on 6460 triple quad mass spectrometer (Agilent, USA) with an electrospray ionization interface (ESI). LC/ESI/MS was conducted in negative-ion mode and

operated under the following conditions: nitrogen gas temperature of 300 °C; dry gas flow rate of 8 L/min; capillary voltage of 3500 V; and nebulizing pressure of 45 psi.

Measurement of wavelength-dependent peak current. A home-made photoelectrochemical apparatus (shown in Figure S12 in the supporting information) was used for the measurement of wavelength-dependent peak currents. The electrochemical detection conditions were the same as described before.

Modification of the AuNPs on a glass slide. AuNPs (50 nm) with an LSPR band centered at ~551 nm were modified on an indium-tin-oxide (ITO) slide for *in situ* dark-field scattering spectroscopy observation. Before modification, the microscope slide was sonicated in acetone for 2 h to remove any dust particles. Then, the slide was thoroughly rinsed with water, blow-dried with nitrogen gas, and treated with a PSD-UV4 ozone system (Novascan 203 Technologies) cleaner for 60 min to further remove organic contaminants from the surface and make the glass hydrophilic. The cleaned slide was then immersed into a freshly prepared diluted solution of AuNPs for 1 h, rinsed with water, and blow-dried with nitrogen gas. Then, the AuNP-functionalized ITO was assembled on a platform as the working electrode. A Pt wire was used as the auxiliary electrode, and a Ag/AgCl was used as the reference. All tests were carried out at room temperature.

Detection of •OH radicals. The experiment was performed on a fluorescence spectrophotometer (RF-5301PC, Shimadzu, Japan). Typically, DCDHF (1.25 mM) was prepared using 0.01 M KOH in a water/ethanol (1:1, v/v) solvent as the stock solution.[36,37] Upon LSPR excitation, the DCDHF stock solution was added into the reaction system. The fluorescence detection was performed after 40-min illumination. The excitation wavelength was 500 nm.

Acknowledgments. This work is supported by grants from the National Natural Science Foundation of China (21327902, 21575163, 21635004, 21675079), and the Natural Science Foundation of Jiangsu Province (BK20151437).

Supporting Information Available:

This material is available free of charge via the Internet at http://pubs.acs.org.

Figure S1-S12 and Table S1. Additional data on illumination responses of different electrodes, UV–vis spectrum of the AuNPs, electrocatalysis of glucose, illumination effect on glucose oxidation at Au disk electrode, HPLC-MS of product, electrochemistry of $Ru(NH_3)_6Cl_3$, illustration of the electron energy distribution in AuNPs, *I-t* curves in glucose solution with or without illumination, *in situ* dark-field electrochemical setup, characterizations of AuNPs, electrochemistry of AuNPs, photoelectrochemical apparatus, and current density of glucose on AuNPs with different diameters.

AUTHOR INFORMATION

Corresponding Author

*E-mail: xhxia@nju.edu.cn.

ORCID

Xing-Hua Xia: 0000-0001-9831-4048

Notes

The authors declare no competing financial interest

REFERENCES

(1) Linic, S.; Christopher, P.; Xin, H.; Marimuthu, A. Catalytic and Photocatalytic Transformations on Metal Nanoparticles with Targeted Geometric and Plasmonic Properties. *Acc. Chem. Res.* **2013**, *46*, 1890-1899.

(2) Chou, L. W.; Shin, N.; Sivaram, S. V.; Filler, M. A. Tunable Mid-Infrared Localized Surface Plasmon Resonances in Silicon Nanowires. *J. Am. Chem. Soc.* **2012**, *134*, 16155-16158.

(3) Xiao, Q.; Jaatinen, E.; Zhu, H. Direct Photocatalysis for Organic Synthesis by Using Plasmonic-metal Nanoparticles Irradiated with Visible Light. *Chem. Asian J.* **2014**, *9*, 3046-3064.

(4) Kale, M. J.; Avanesian, T.; Christopher, P. Direct Photocatalysis by Plasmonic Nanostructures. *ACS Catal.* **2014**, *4*, 116-128.

(5) Zhang, H.; Govorov, A. O. Optical Generation of Hot Plasmonic Carriers in Metal Nanocrystals: the Effects of Shape and Field Enhancement. *J. Phys. Chem. C* **2014**, *118*, 7606-7614.

(6) Nie, S.; Emory, S. R. Probing Single Molecules and Single Nanoparticles by Surface-Enhanced Raman Scattering. *Science* **1997**, *275*, 1102-1106.

(7) Moskovits, M. Surface-Enhanced Raman Spectroscopy: a Brief Retrospective. *J. Raman Spectroscopy* **2005**, *36*, 485-496.

(8) Atwater, H. A.; Polman, A. Plasmonics for Improved Photovoltaic Devices. *Nat. Mater.* **2010**, *9*, 205-213.

(9) Kuhn, S.; Hakanson, U.; Rogobete, L.; Sandoghdar, V. Enhancement of Single-Molecule Fluorescence Using a Gold Nanoparticle as an Optical Nanoantenna. *Phys. Rev. Lett.* **2006**, *97*, 017402.

(10) Jain, P. K.; Huang, X.; El-Sayed, I.; El-Sayed, H. M. A. Noble Metals on the Nanoscale: Optical and Photothermal Properties and Some Applications in Imaging, Sensing, Biology, and Medicine. *Acc. Chem. Res.* **2008**, *41*, 1578-1586.

(11) Larsson, E. M.; Langhammer, C.; Zoric, I.; Kasemo, B. Nanoplasmonic Probes of Catalytic Reactions. *Science* **2009**, *326*, 1091-1094.

(12) Schuller, J. A.; Barnard, E. S.; Cai, W. S.; Jun, Y. C.; White, J. S.; Brongersma, M. L. Nanoplasmonic Probes of Catalytic Reactions. *Nat. Mater.* **2010**, *9*, 193-204.

(13) Brongersma, M. L.; Halas, N. J.; Nordlander, P. Plasmon-Induced Hot Carrier Science and Technology. *Nat. Nanotechnol.* **2015**, *10*, 25-34.

(14) Linic, S.; Aslam, U.; Boerigter, C.; Morabito, M. Photochemical Transformations on Plasmonic Metal Nanoparticles. *Nat. Mater.* **2015**, *14*, 567-576.

(15) Linic, S.; Christopher, P.; Ingram, D. B. Plasmonic-Metal Nanostructures for Efficient Conversion of Solar to Chemical Energy. *Nat. Mater.* **2011**, *10*, 911-921.

(16) Chen, X.; Zhu, H. Y.; Zhao, J. C.; Zheng, Z. F.; Gao, X. P. Visible-Light-Driven Oxidation of Organic Contaminants in Air with Gold Nanoparticle Catalysts on Oxide Supports. *Angew. Chem. Int. Ed.* **2008**, *47*, 5353-5356.

(17) Christopher, P.; Xin, H.; Linic, S. Visible-Light-Enhanced Catalytic Oxidation Reactions on Plasmonic Silver Nanostructures. *Nat. Chem.* **2011**, *3*, 467-472.

(18) Christopher, P.; Xin, H.; Marimuthu, A.; Linic, S. Singular Characteristics and Unique Chemical Bond Activation Mechanisms of Photocatalytic Reactions on Plasmonic Nanostructures. *Nat. Mater.* **2012**, *11*, 1044-1050.

(19) Mukherjee, S.; Zhou, L. N.; Goodman, A. M.; Large, N.; Ayala-Orozco, C.; Zhang, Y.; Nordlander, P.; Halas, N. J. Hot-Electron-Induced Dissociation of H_2 on Gold Nanoparticles Supported on SiO_2. *J. Am. Chem. Soc.* **2014**, *136*, 64-67.

(20) Mukherjee, S.; Libisch, F.; Large, N.; Neumann, O.; Brown, L. V.; Cheng, J.; Lassiter, J. B.; Carter, E. A.; Norlander, P. N.; Halas, J. Hot Electrons Do the Impossible: Plasmon-Induced Dissociation of H_2 on Au. *Nano Lett.* **2013**, *13*, 240-247.

(21) Robatjazi, H.; Bahauddin, S. M.; Doiron, C.; Thomann, I. Direct Plasmon-Driven Photoelectrocatalysis. *Nano Lett.* **2015**, *15*, 6155-6161.

(22) Huang, Y. F.; Zhang, M.; Zhao, L. B.; Feng, J. M.; Wu, D. Y.; Ren, B.; Tian, Z. Q. Activation of Oxygen on Gold and Silver Nanoparticles Assisted by Surface Plasmon Resonances. *Angew. Chem. Int. Ed.* **2014**, *53*, 2353-2357.

(23) Shi, Y.; Wang, J.; Wang, C.; Zhai, T. T.; Bao, W. J.; Xu, J. J.; Xia, X. H.; Chen, H. Y. Hot Electron of Au Nanorods Activates the Electrocatalysis of Hydrogen Evolution on MoS_2 Nanosheets. *J. Am. Chem. Soc.* **2015**, *137*, 7365-7370.

(24) Kim, K.; Lee, S. H.; Choi, J. Y.; Shin, K. S. Fe^{3+} to Fe^{2+} Conversion by Plasmonically Generated Hot Electrons from Ag Nanoparticles: Surface-Enhanced Raman Scattering Evidence. *J. Phys. Chem. C* **2014**, *118*, 3359-3365.

(25) Zhu, H. Y.; Ke, X. B.; Yang, X. Z.; Sarina, S.; Liu, H. W. Reduction of Nitroaromatic Compounds on Supported Gold Nanoparticles by Visible and Ultraviolet Light, *Angew. Chem. Int. Ed.* **2010**, *49*, 9657-9661.

(26) Frens, G. Controlled Nucleation for the Regulation of the Particle Size in Monodisperse Gold Suspensions. *Nature* **1973**, *241*, 20-22.

(27) Luo, W. J.; Zhu, C. F.; Su, S.; Li, D.; He, Y.; Huang, Q.; Fan, C. H. Self-Catalyzed, Self-Limiting Growth of Glucose Oxidase-Mimicking Gold Nanoparticles. *ACS Nano* **2010**, *4*, 7451-7458.

(28) Li, K.; Wang, K.; Qin, W. W.; Deng, S. H.; Li, D.; Shi, J. Y.; Huang, Q.; Fan, C. H. DNA-Directed Assembly of Gold Nanohalo for Quantitative Plasmonic Imaging of Single-Particle Catalysis. *J. Am. Chem. Soc.* **2015**, *137*, 4292-4295.

(29) Furube, A.; Du, L.; Hara, K.; Katoh, R.; Tachiya, M. Ultrafast Plasmon-Induced Electron Transfer From Gold Nanodots into TiO_2 Nanoparticles. *J. Am. Chem. Soc.* **2007**, *129*, 14852-14853.

(30) McFarland, E. W.; Tang, J.; A Photovoltaic Device Structure Based on Internal Electron Emission. *Nature* **2003**, *421*, 616-618.

(31) Govorov, A. O.; Zhang, H.; Gun'ko, Y. K. Theory of Photoinjection of Hot Plasmonic Carriers From Metal Nanostructures into Semiconductors and Surface Molecules. *J. Phys. Chem. C* **2013**, *117*, 16616-16631.

(32) Novo, C.; Funston, A. M.; Mulvaney, P. Direct Observation of Chemical Reactions on Single Gold Nanocrystals Using Surface Plasmon Spectroscopy. *Nat. Nanotechnol.* **2008**, *3*, 598-602.

(33) Knight, M. W.; Wu, Y.; Lassiter, J. B.; Nordlander, P.; Halas, N. J. Substrates Matter: Influence of an Adjacent Dielectric on an Individual Plasmonic Nanoparticle. *Nano Lett.* **2009**, *9*, 2188-2192.

(34) Manjavacas, A.; Liu, J. G.; Kulkarni, V.; Nordlander, P. Plasmon-Induced Hot Carriers in Metallic Nanoparticles. *ACS Nano* **2014**, *8*, 7630-7638.

(35) Simon, T.; Bouchonville, N.; Berr, M. J.; Vaneski, A.; Adrovic, A.; Volbers, D.; Wyrwich, R.; Döblinger, M.; Susha, A. S.; Rogach, A. L.; Jäckel, F.; Stolarczyk, J. K.; Feldmann, J. Redox Shuttle Mechanism Enhances Photocatalytic H_2 Generation on Ni-Decorated CdS Nanorods. *Nat. Mater.* **2014**, *13*, 1013-1018.

(36) Wang, J.; Wang, H. S.; Wang, K.; Wang, F. B.; Xia, X. H. Ice Crystals Growth Driving Assembly of Porous Nitrogen-Doped Graphene for Catalyzing Oxygen Reduction Probed by *in situ* Fluorescence Electrochemistry. *Sci. Rep.* **2014**, *4*, 6723.

(37) Wang, J.; Wang, K.; Wang, F. B.; X. H. Xia, Bioinspired Copper Catalyst Effective for Both Reduction and Evolution of Oxygen. *Nat. Commun.* **2014**, *5*, 5285.

(38) Slot, J. W.; Geuze, H. J. A New Method of Preparing Gold Probes for Multiple-Labeling Cytochemistry. *Eur. J. Cell. Biol.* **1985**, *38*, 87-93.